npj | climate and atmospheric science

Article

Published in partnership with CECCR at King Abdulaziz University

https://doi.org/10.1038/s41612-025-01014-y

Global coupled dynamics of tropical easterly waves and tropical cyclone genesis

Check for updates

Xueqing Du[1], Jung-Eun Chu[1] ✉, Fei-Fei Jin[2] & Hung Ming Cheung[3]

Tropical easterly waves (TEWs) are westward-moving waves often within trade winds but occur ubiquitously in the tropics and play a significant role in the genesis of tropical cyclones (TCs). They are well-known as primary precursors of TCs in the Atlantic, yet their global relationship with TCs has been less explored. This study, for the first time, presents the global distribution of TEW activity using a combined thermodynamic and dynamic framework based on 6-hourly Outgoing Longwave Radiation and curvature vorticity. We then demonstrate that TEWs play a dominant role in approximately 22–71% of global TC genesis, with their highest impacts in the North Atlantic (71%) and Western Pacific (54%). We further identify that TEWs, in their general coupling with TC genesis dynamics, act to intensify TC convection and vorticity in all TC main development regions, albeit the vorticity enhancement is relatively weaker in the North Atlantic. To understand the cross-basin differences in this general TEW-TC relationship, we further investigated background conditions for TC genesis in each basin and found an additional dry environment constraint in the Atlantic TC genesis, yet still delineating the critical role of TEWs in TC development.

Tropical easterly waves (TEWs) are tropical waves that exist in tropical and subtropical regions. They propagate from east to west with a wavelength of about 3000 kilometers and a speed of 7–8 m/s[1–5]. Over the north Africa and north Atlantic (AL), these waves are known as African easterly waves (AEWs). AEWs are generated via instability mechanisms along the African easterly jet[6,7], which features an easterly wind reaching around 15 m/s at nearly 600–700 hPa[8]. It has been well-established that convective activities, including rainfall events and mesoscale convective systems in the Sahara Desert, often occur along the troughs of AEWs[9–16]. Mesoscale convective systems play a significant role in AEW growth and, ultimately, hurricane genesis[17]. AEWs are commonly considered the main precursors of hurricane development in the AL, accounting for up to 75% of hurricanes and 85% of intense hurricanes in that region[18–20]. However, whether the presence of AEWs is a necessary condition for hurricane developments is still debated[21–23].

Outside of the Atlantic region, TEWs also exist along the intertropical convergence zone (ITCZ). For example, TEWs in the eastern Pacific (EP) region have different sources, including the downstream AEWs from the AL[24] and local generation through interaction with the Caribbean low-level jet[25]. To distinguish TEWs from other tropical waves, a spatiotemporal filter method[26] is often applied to convective variables such as rainfall[27,28] and outgoing longwave radiation (OLR)[29,30]. In general, tropical waves in the tropical ocean are mainly classified into 5 groups: tropical depression (TD)-type waves, mixed Rossby-gravity waves, Equatorial Rossby waves, Kelvin waves, and Madden-Julian Oscillation[27–29,31]. Among these, TD-type waves are specifically westward-propagating waves with a zonal number of 6–20 and a period of 2–10 days, and these waves are also considered TEWs. Using the filtered multi-satellite rainfall estimates, studies have shown that TD-type waves are the dominant source of tropical cyclone (TC) genesis, accounting for over 60% of TCs in the western Pacific (WP), EP, and north Indian Ocean (NI), and over 80% in the AL, while around 40% in the south Indian Ocean (SI) and south Pacific (SP).

Some TEWs are dry in nature and, therefore, are better identified by dynamical variables, such as relative vorticity (RV)[25,32] and curvature vorticity (CV)[32–34], than convective variables. The CV, in particular, is calculated by subtracting shear vorticity (SV) from the RV (See *Methods*), which provides a more accurate measure of the rotational motion of the TEWs[35] (Supplementary Fig. S1). Some attempts have been made to identify TEWs using both convective and dynamical fields. For example, Torres and Thorncroft[36] effectively diagnosed TEW activities by utilizing TD-filtered OLR and 2–10 days bandpass filtered CV focusing only over the EP.

[1]School of Energy and Environment, City University of Hong Kong, Hong Kong, China. [2]Department of Atmospheric Sciences, School of Ocean and Earth Science and Technology, University of Hawaii at Mānoa, Honolulu, HI, USA. [3]Severe Storm Research Center, Ewha Womans University, Seoul, Republic of Korea. ✉e-mail: jungeun.chu@cityu.edu.hk

Recently, Hollis et al.[4] made the first attempt to detect and track TEWs globally at 700 hPa and 850 hPa using CV. Their study shows that TEWs are active over the whole subtropical basins, including AL, EP, WP, NI, SI, and SP. While the primary regions of TEWs activity resemble those of TC genesis, whether and how TEWs are significantly linked to TCs outside of the AL remains unresolved.

In this study, our goal is to investigate, for the first time, the global distribution of TEWs and their role in TC genesis using both convective (i.e., OLR) and dynamic variables (i.e., CV) by the observation from the fifth generation ECMWF reanalysis (ERA5)[37] and the International Best Track Archive for Climate Stewardship[38,39] during 1980–2023. We define TC active seasons as June to October (JJASO) for the boreal summer and December to April (DJFMA) for the austral summer.

Results

The global distribution of TEWs and TC genesis

Figure 1A, B shows the global distribution of convective and dynamical variables used to detect TEW activity, as well as locations of TC genesis. In boreal summer and autumn, TEW convection (shown by the blue lines in Fig. 1A) is located along the entire tropics, typically south of 20°N. The convection centers extend northward to 30°N in the AL and WP and southward to 10°S in the SI and SP. During the austral TC season, convection is active in the tropical SI and SP, as well as south of 10°N in the Northern Hemisphere (Fig. 1B). Those convective areas coincide with the boreal summer ITCZ and West African Monsoon, and austral summer South Pacific Convergence Zone.

The dynamical TEW active regions (i.e., TD-filtered CV at 900 hPa) are mainly located north of 10°N in the boreal TC season and south of 10°S in the austral TC season with the highest values over the western boundaries of WP and AL, as well as the southeastern edge of the EP (red lines in Fig. 1A, B). It is interesting to note that the overlapping regions where the convective and dynamical metrics indicate high TEW activity are also where the majority of TCs are generated. Motivated by the definition of main development region (MDR) in the AL[40], here we expand this definition into all six active TEW basins globally (black boxes in Fig. 1A, B).

Figure 1C–H shows the scatter plot of two variables (i.e., CV at 900 hPa and OLR) during TC genesis, as well as their corresponding probability density functions. The percentage of TCs linked to negative OLR and positive CV anomalies ranges from 56–88% across the different MDRs analyzed. Specifically, AL accounts for 88%, followed by WP and EP with 79%. NI, SI, and SP are ordered with 77%, 77%, and 56%, respectively. On average, about 80% of global TC genesis are associated with TEW indicators. This result is about 20% higher than previous studies that only used convective metrics[28] and eddy kinetic energy metrics[19], and about 30% higher than using OLR and RV metrics over the WP[31]. Moreover, our result is about 10% higher than westward-moving equatorial waves, including mixed Rossby-gravity (MRG) waves and mode number 1 and 2 Rossby waves, defined by dynamical fields in each basin[41]. The higher percentages obtained in this study can be attributed to: 1) using CV instead of RV as the dynamical variable, 2) incorporating both dynamic and convective variables, and 3) applying a narrower 6–20 westward wavenumber band for spatial filtering. This demonstrates that using the combined convective and dynamical metrics employed in this study is more effective at detecting TC genesis in relation to TEW activity than other previous methods, while TEWs defined in this study are in line with different types of westward-moving Rossby waves[42].

To conduct a more rigorous investigation of the relationship between TEWs and TC genesis, we define the "coupled" cases as those meeting the one-standard deviation (STD) criteria of OLR anomaly (-10 W m^{-2}) and CV anomalies ($\pm 0.3 \times 10^{-5}$ s^{-1}, positive in the Northern Hemisphere and negative in the Southern Hemisphere). All other cases not meeting this one-STD criteria are defined as "not-coupled" cases. Under this definition, 22–71% of TCs are coupled with TEWs across the different basins, with the highest value in AL (71%) and WP (54%) (Fig. 1C–H). More than 50% of TCs are coupled with TEWs globally.

Previous studies have generally detected and tracked TEWs using CV at 850 hPa and 700 hPa[4,34,36,43–45]. To understand the vertical structure of TEW activities, we calculated TD-filtered CV across various atmospheric levels from 200 hPa to 1000 hPa in each MDR (Supplementary Fig. S2). In most basins, CVs during TC genesis are higher below 500 hPa, with maximum values typically occurring at 900 hPa in conjunction with TEWs. Consequently, we chose 900 hPa as the primary level for assessing TEW-TC activity. We further examine the sensitivity of selecting different levels for CV at 850 hPa (Supplementary Fig. S3) and 700 hPa (Supplementary Fig. S4) and find that the quantitatively similar results convince our TEWs distribution.

It is interesting to note that TEW-TC coupled events do not exhibit a clear geographical preference within areas that meet the criteria for both OLR and CV, except for the AL basin (Supplementary Fig. S5). Additionally, most TC genesis events north of 30° latitude in the AL and WP basins are associated with "not-coupled" cases, meaning they occurred without a corresponding TEW event (Supplementary Fig. S5B). Furthermore, TC genesis events during the non-TC season, such as in the Southern Hemisphere in Supplementary Fig. S5B and those in the Northern Hemisphere in Supplementary Fig. S5D, are also associated with "not-coupled" cases. Previous studies have used a combination of 4–5 large-scale variables to create an empirical "Genesis Potential Index" to represent TC genesis locations. However, results from this study suggest that two parameters – OLR and CV – can explain most of TC genesis with the exception of northwestern AL, and those events might be associated with non-tropical characteristics[46].

The impact of TEWs on TC genesis and tracks

We here delve into the impact of TEWs on TC genesis convective and dynamical structures from the composite patterns of TC horizontal OLR (Fig. 2, Supplementary Figs. S6 and S7) and CV (Fig. 3, Supplementary Figs. S8 and S9). During TC genesis, TEWs exhibit strong negative OLR and cyclonic CV anomalies across all the basins. However, the magnitude and structure of these OLR and CV anomalies are subtly different between the various ocean basins. The convection structures exhibit a northeast-southwest tilt in the Northern Hemisphere (Fig. 2A–D) and a northwest-southeast in the Southern Hemisphere (Fig. 2E, F). This horizontal tilting of convection structures in opposite directions between the hemispheres reflects the cyclonic (i.e., counterclockwise in the Northern Hemisphere and clockwise in the Southern Hemisphere) rotation of the TEW convection, affected by the direction of TC winds. The coupled TEW-TC convections are strongest in the AL, followed by NI and WP, but relatively weaker in the EP and SI and weakest in the SP basins (Fig. 2A–F, Supplementary Figs. S6A–F and S7A–F).The dynamical fields related to the TEWs show similarly circular but tilted patterns centered around the TC genesis locations (Fig. 3A–F, Supplementary Figs. S8A–F and S9A–F). Differently from the magnitude of OLR, the composite CV fields display stronger vorticity anomalies in the NI, WP, SI, and SP basins while relatively weaker in the EP and SP.

To illustrate the impact of TEWs on TC genesis in each basin, we distinguish between TC genesis events that are coupled with TEWs versus those that occur without coupling to TEWs. The cases where TC genesis is coupled with TEWs exhibit much stronger convection compared to non-coupled cases with OLR anomalies more than 5 times larger in all basins (Fig. 2M–R, Supplementary Figs. S6M–R and S7M–R). This suggests that the interaction between TEWs and TCs leads to enhanced convection and potentially more favorable conditions for TC intensification versus TC genesis that occurs independently of the large-scale TEW circulations. In addition to the enhanced convection, TEWs also act to magnify TC dynamical structures of the TC genesis (Fig. 3M–R, Supplementary Figs. S7M–R and S8M–R). TCs generated with TEWs show significantly stronger CV fields than without TEWs. This intensification effect in dynamical fields is prominent, with about 60–80% enhancement in the NI, WP, EP, SI, and SP, but is weakest, only 50%, in the AL.

Furthermore, TEWs, as westward-moving waves, can effectively guide TCs to move westward after genesis (Fig. 4, Supplementary Figs. S10 and S11). The ratio of TCs moving westward versus poleward in the first

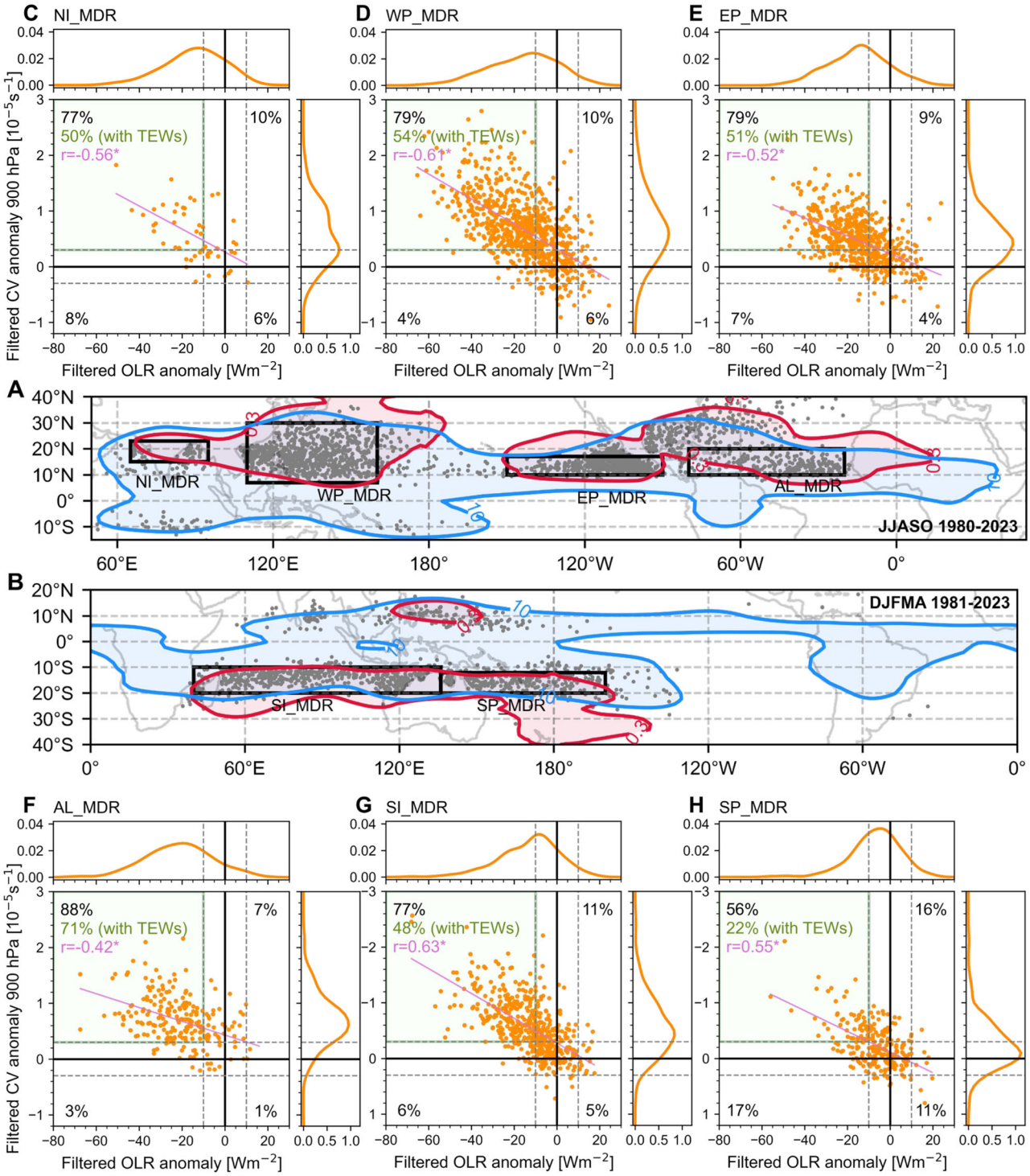


Fig. 1 | The global distribution of tropical easterly wave (TEW) activity climatology and tropical cyclone (TC) genesis and their relationship. A The climatology of tropical depression (TD)-filtered Outgoing Longwave Radiation (OLR) seasonal standard deviation (STD; blue contours and shading, in Wm^{-2}) and TD-filtered curvature vorticity (CV) at 900 hPa seasonal STD (red contours and shading, in $10^{-5}s^{-1}$) for JJASO during 1980–2023, and all TC genesis locations (gray dots). **B** As in (**A**), but for DJFMA during 1981–2023. The black boxes enclose the main development regions (MDRs) in the north Indian Ocean (NI), western Pacific (WP), eastern Pacific (EP), Atlantic (AL), south Indian Ocean (SI), and south Pacific (SP). **C**–**H** Scatter plots and probability density function (PDF) plots of TD-filtered OLR anomaly (in Wm^{-2}) and TD-filtered CV anomaly at 900 hPa (in 10^{-5} s^{-1}) radially averaged (500 km) for each TC domain during TC genesis in (**C**) NI, (**D**) WP, (**E**) EP, (**F**) AL, (**G**) SI, and (**H**) SP MDRs. The horizontal (vertical) solid lines indicate the regional averaged TD-filtered CV at 900 hPa (TD-filtered OLR) anomaly value, and dashed gray lines are the corresponding ±1 STD criteria for each variable (±10 W m^{-2} for OLR and ±0.3 ×10^{-5} s^{-1} for CV). The numbers in black represent the percentages of TC genesis cases in each quadrant defined by the regional average values to the total. The number in green in the upper-left quadrant indicates the percentage of coupled TEW-TC cases. The purple line shows the linear relation between OLR and CV anomaly for all TC cases in each basin and the correlation coefficient is shown in purple with * indicating the significance at the 99% confidence levels.

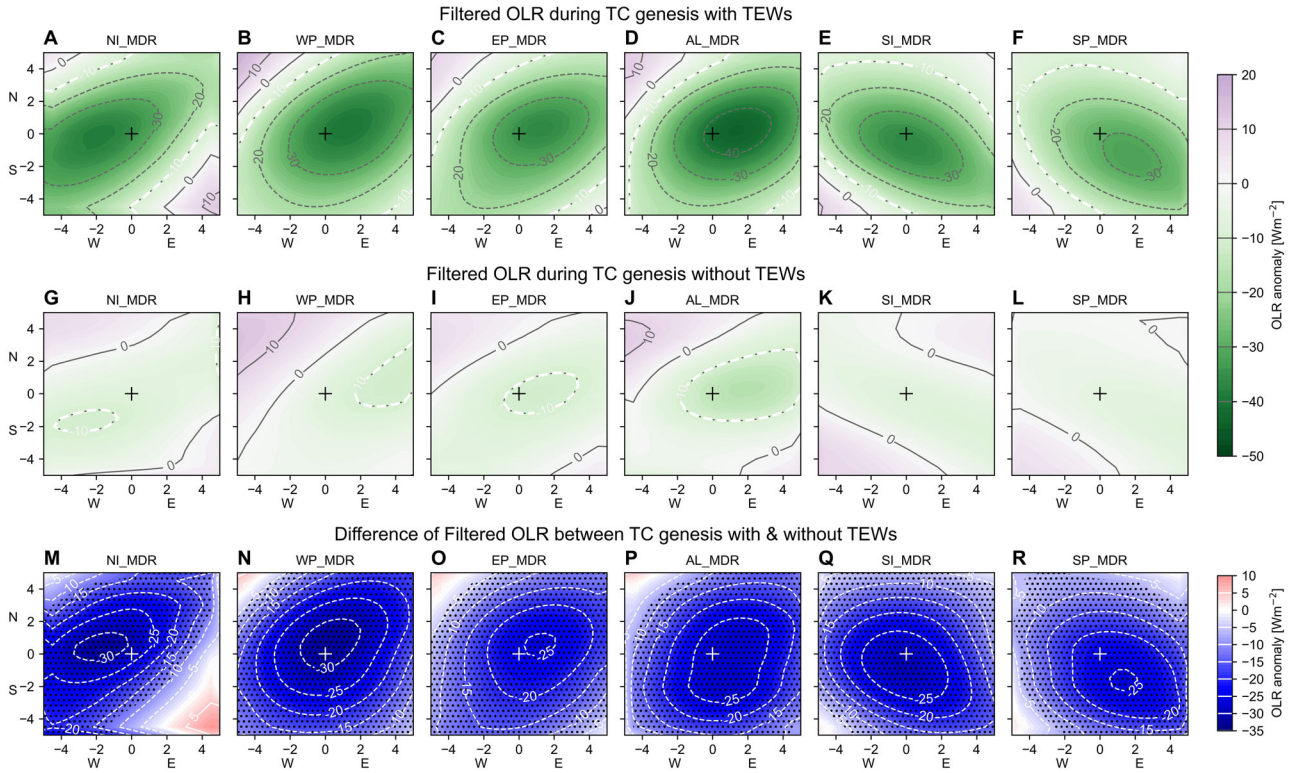


Fig. 2 | TEWs' impact on TC convective structures during genesis. Storm-centered composites of TD-filtered OLR anomaly (in W m^{-2}) for TC domains during TC genesis (**A**–**F**) with and (**G**–**L**) without TEWs in the NI, WP, EP, AL, SI, and SP MDRs, respectively. The "coupled" case classification is based on one standard deviation of OLR and CV at 900 hPa. **M**–**R** show the corresponding differences for each basin, and the dotted shadings denote the significant differences at the 95% confidence levels. The origin represents the location of all composited TC genesis cases marked as the plus marker.

six hours after TC genesis (i.e., Northwards in the Northern Hemisphere and southwards in the Southern Hemisphere) is 78% vs 22% for those coupled to TEWs (Fig. 4A). On the other hand, this ratio shows negligible difference (53% vs 47%) for those not coupling to TEWs (Fig. 4B). Dunkerton et al.[47] emphasized that Kelvin cat's eye structure plays a critical role on TC generation from TEWs and their in-phase movement in the AL and EP. Recently, Núñez Ocasio et al.[17] also found that convective systems over Africa coupled to developing TEWs show in-phase moving with wave troughs. Our results confirm that the guiding effect of TEWs on the initial movement direction of TCs is globally distributed.

In summary, TEWs act to intensify TC convection and vorticity, although the vorticity enhancement in the AL is relatively weaker. This globally distributed TEW-TC coupling structure also guides TCs to have a greater chance of moving westwards after genesis. The remaining question is why there is less intensification in the TC dynamical fields in the AL. Our hypothesis is that AL MDRs have unfavorable environmental conditions for TC genesis, and therefore, storms require an environment similar to the active cyclonic regions of TEWs in order to survive.

Impact of basin-dependent environmental conditions on TEW-TC interactions

To examine how the background environmental conditions in each basin impact the coupled structures of TEWs and TCs, we analyze the evolutional background condition during 18, 12, and 6 h prior to and during TC genesis, including vertical wind shear (VWS), relative humidity at 700 hPa, and mixing ratio at 925 hPa (Fig. 5, Supplementary Figs. S12 and S13). Interestingly, we find apparent regional differences in moisture conditions across the different basins, while the difference between coupled and non-coupled to TEWs is relatively minor. Moreover, the variations in both moisture conditions (i.e., relative humidity and mixing ratio) and dynamical conditions (i.e., VWS) leading up to TC genesis do not consistently show statistically significant differences between coupled and non-coupled cases (Fig. 5). This suggests the regional background conditions have a greater influence on the characteristics of the coupled TEW-TC structures than the direct association of TCs with TEWs. Specifically, the VWS values averaged within 500 km of the TC center are below 13 m/s in all basins, with the lowest value at 7–8 m/s in the EP, 9–10 m/s in the AL and WP, and 10–13 m/s in the SP, SI, and NI. Despite these regional average differences, VWS values on TC centers remain well below 10 m/s in all 6 basins, regardless of TEW coupling (Supplementary Figs. S14 and S15), which are favorable in TC development[48,49]. However, the exceptionally dry environment in the AL, reflected by relative humidity below 70% at 700 hPa and mixing ratio under 16.5 g/kg at 925 hPa 18 h prior to TC genesis, shows an adverse environment for TC genesis in this basin (Fig. 5C–F, Supplementary Figs. S12C–F and S13C–F). The most noticeable change is the increase in relative humidity in the AL reaching about 70% as it approaches the TC genesis, with this increase being more pronounced in coupled cases (Fig. 5C, D). In addition, this enhancement of favorable moisture environments in the AL is linked to the westward moving system, while those are not apparent in other basins (Supplementary Figs. S16–19).

Our results demonstrate that storms in the AL MDR need environments like TEWs to protect their convective aggregation, especially under unfavorable moisture conditions due to the Saharan desert[47,50–52]. This also explains a notably high percentage (71%) of TCs in the AL associated with TEW environments (Fig. 1F). A recent quantitative study on an AL hurricane Helene (2006) highlighted the important role of moisture in TC genesis from an AEW behaving as a moisture mode[51]. Our result further suggests the critical role of moisture conditions in influencing the cross-basin TEW-TC coupled dynamical structures. It is well-studied that AEWs are initiated by the shear instability of the African easterly jet, specifically the evolution of baroclinic and barotropic conversions[53,54]. However, whether this dynamical instability is strong enough to generate waves is still debated[55–57]. In contrast, TEWs in the WP, also called TD-waves or summertime synoptic-scale waves, are considered to originate from wave

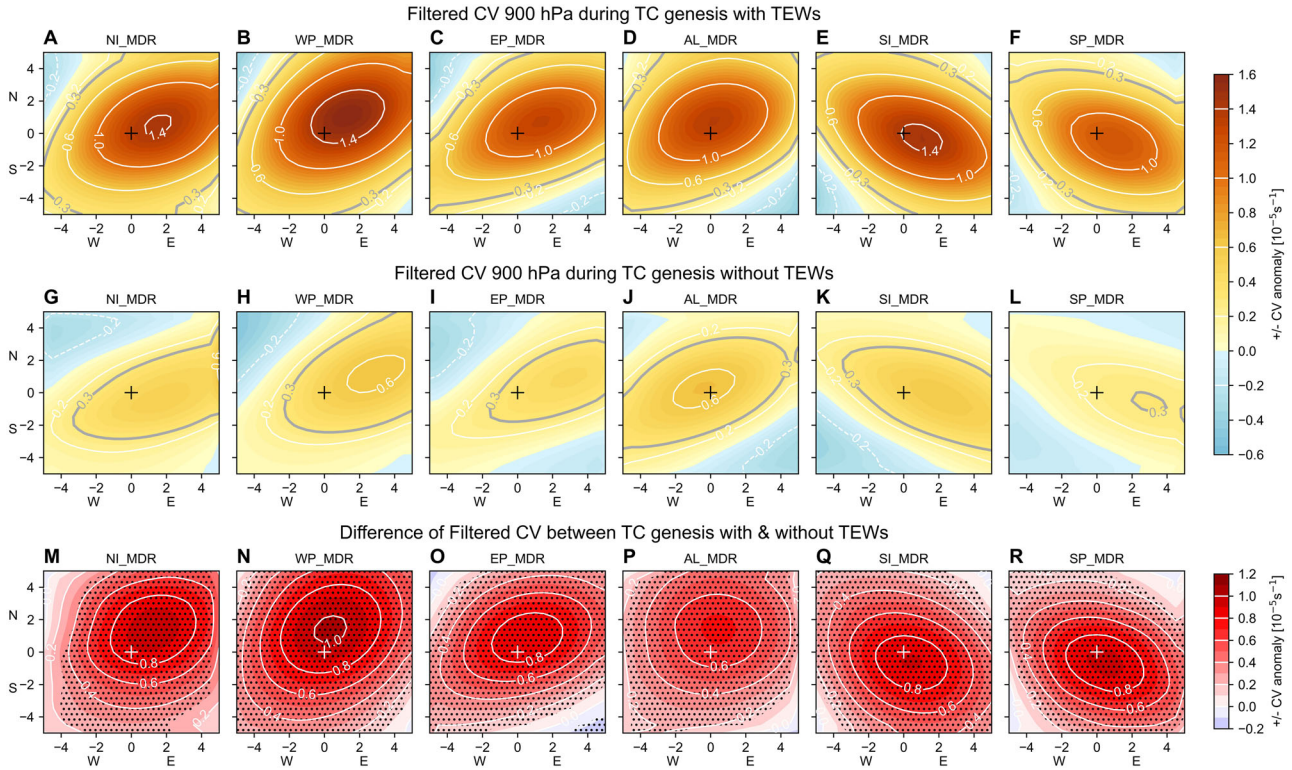


Fig. 3 | TEWs' impact on TC vorticity structures during genesis. As in Fig. 2, but for TD-filtered CV anomaly at 900 hPa (in $10^{-5}s^{-1}$) for TC domains during TC genesis (**A**–**F**) with and (**G**–**L**) without TEWs, and (**M**–**R**) their differences in the NI, WP, EP, AL, SI, and SP MDRs. The CV value for the SI and SP is multiplied with −1 (**E**, **F**, **K**, and **L**).

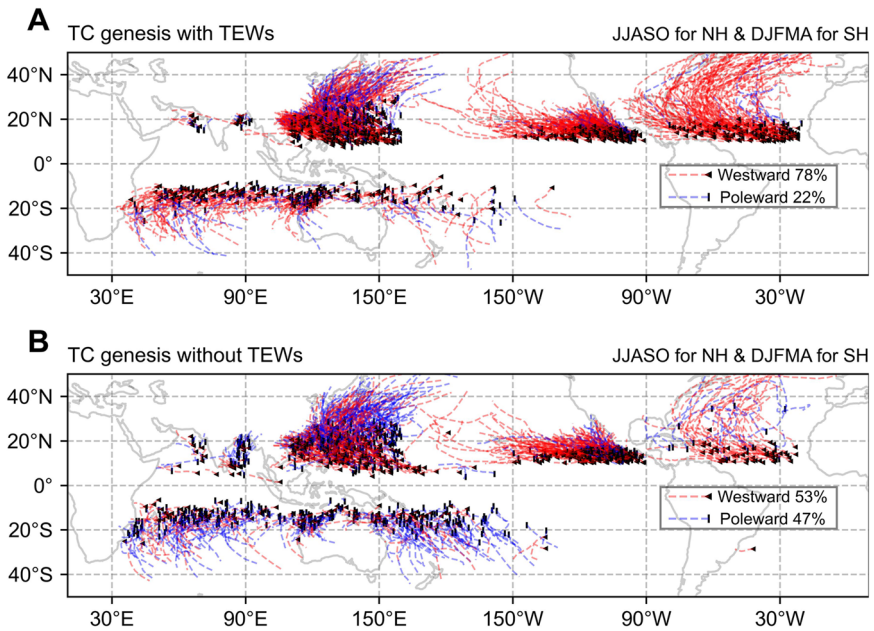


Fig. 4 | TEWs' impact on TC movement direction after genesis. A Track of TCs generated with TEWs in MDRs for JJASO during 1980–2023 in the Northern Hemisphere and for DJFMA during 1981–2023 in the Southern Hemisphere. **B** As in (**A**), but for TC genesis without TEWs. The "coupled" case classification is based on one standard deviation of OLR and CV at 900 hPa. The triangle marker shows the TC genesis location and red dashed line shows the corresponding track for TC genesis with TEWs cases. The bar marker and blue dashed line indicates TC genesis without TEWs cases. The global percentages of these two groups are shown in the legend box.

accumulation of convective eddy flux[58–60]. Our findings of differences in dry and wet background conditions between the AL and other basins further imply the cross-basin distinct mechanisms of TEWs, although less is known about the EP, Indian Ocean, and Southern Hemisphere.

Discussion

This study introduces a framework that combines OLR and CV to represent TEW activities and their coupled structures with TC genesis globally. We find that approximately 80% of TCs globally are associated with TEWs based on our metrics. Considering the OLR and CV one-STD criteria, about 50% of TC genesis cases are coupled with TEW events, with 50%, 54%, 51%, 71%, 48%, and 22% in the NI, WP, EP, AL, SI, and SP MDRs, respectively. TEWs typically act to amplify the convective and dynamical structures during TC genesis. However, there is a relatively weak intensification of the coupled TEW-TC dynamical structures in the AL due to the limitation of the dry background environment.

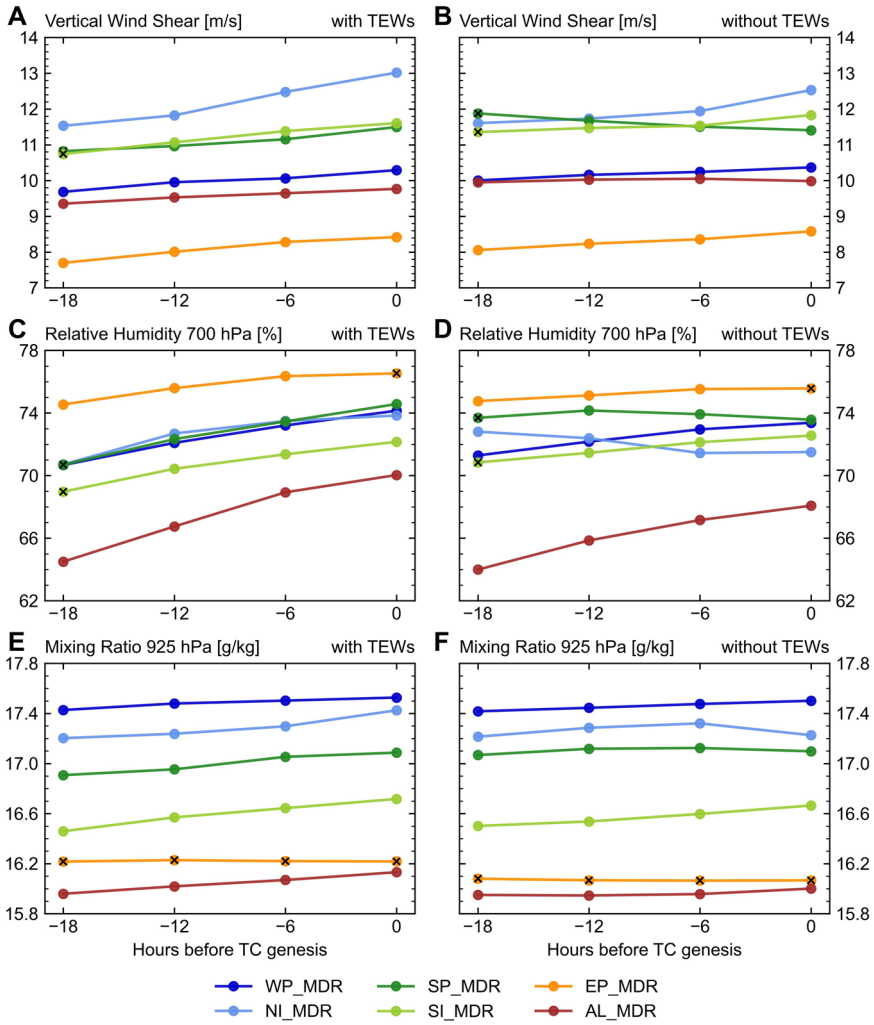


Fig. 5 | Time evolution of environment factors related to TC genesis. A The time series of case-ensembled 500 km radially regional averaged vertical wind shear (in m/s) with the time prior to TC genesis (18, 12, 6, and 0) for TC cases generated with TEWs in each basin. **B** As in (**A**), but for TC cases without TEWs. **C, D** as in (**A**, **B**), but for relative humidity at 700 hPa (in %). **E**, **F** as in (**A**, **B**), but for mixing ratio at 925 hPa (in g/kg). The center of the 500 km averaging is always placed on where and when TC genesis. Cross markers denote the statistically differences between cases with and without TEWs at the 95% confidence levels.

This study spotlights the role of moisture in TEWs as a key factor in tropical variability in the AL[61]. However, the source of moisture and the intricate relationship between moisture and wave-vortex structure should be further investigated in individual case studies. For example, Núñez Ocasio and Rios-Berrios[51] demonstrated that boundary layer moisture flux was crucial for the genesis of Hurricane Helene (2006). Another recent study by Núñez Ocasio et al.[62] proposed that the West African Monsoon plays a direct role in TC genesis due to prolonged interaction with monsoon moisture and enhanced vortex stretching[17,63] in eastern Africa. On the other hand, a convection-permitting model experiment suggested that intense monsoonal flow can decouple convection from AEW by slowing down the westward propagation of the waves[52]. Our AL MDR is located north of West African Monsoon precipitation, indicating that the monsoon indirectly supports TC genesis by providing precursors from monsoon trough and shear in the easterly monsoon regions (Supplementary Fig. S20). Therefore, understanding this interaction is essential for improving predictions of TC behavior in the AL.

This study offers a comprehensive investigation of the TEWs-TCs interaction on a global scale. In terms of TEWs, global representation of their characteristics, such as amplitude, frequency, and phase speed, will open up for further investigations. Additionally, understanding the mechanisms that drive TEW generation in different basins remains an important issue. A promising approach to address this involves quantifying the relative contribution of barotropic-baroclinic instability and moisture mode dynamics to TEW formation. Moreover, assessing the ability of numerical models to accurately capture the TEWs and their impacts on TCs is necessary for better detection and prediction of natural disasters.

Materials and methods

Observational data

This study uses 6-hourly (0, 6, 12, and 18 UTC) total net thermal radiation from OLR from the fifth generation European Centre for Medium-Range Weather Forecasts (ECMWF) reanalysis (ERA5)[64] with a horizontal resolution of 0.25° × 0.25° latitude by longitude. The OLR (unit: W m^{-2}) is equal to the negative of total net thermal radiation (unit: J m^{-2}) after dividing by the accumulation period (3600 s). The 6-hourly (0, 6, 12, and 18 UTC) u-wind and v-wind from 1000 to 200 hPa used to get curvature vorticity (CV), relative vorticity (RV), and shear vorticity (SV) were also obtained from the ERA5[37]. The TC best track data was provided by NOAA International Best Track Archive for Climate Stewardship (IBTrACS)[38,39] at 6-hourly intervals. We use TCs' location (latitude and longitude) and their intensity (the maximum 1-min sustained wind speed), which are recorded by the forecast agencies in the USA. We define the TC genesis time and location when and where the storm intensity reaches 34 kt. For the composites of TC genesis background conditions, including VWS, relative humidity, and mixing ratio, we also use the 6-hourly data from ERA5[37] with a horizontal resolution of 0.25° × 0.25° latitude by longitude for the listed variables: u-wind, relative humidity, and specific humidity. The VWS is defined as the difference of the u-wind vector between 200 and 850 hPa.

CV calculation

In this study, we calculate the RV, SV, and CV using u-wind and v-wind from the reanalysis dataset at multiple pressure levels. Viúdez and Haney[65] list the equations in natural coordinates, and here we give corresponding expressions for the gridded data in rectangular coordinates. The vertical

component of RV is the sum of SV and CV, i.e.

$$\zeta = -\nabla_h \cdot \left(\left|\vec{V}\right| \vec{n}\right) = \left(-\nabla_h \left|\vec{V}\right| \cdot \vec{n}\right) + \left(-\left|\vec{V}\right| \nabla_h \cdot \vec{n}\right) = \zeta^s + \zeta^c \tag{1}$$

where $\nabla_h = (\partial_x, \partial_y)$ is the isobaric gradient operator, $\vec{V} = (u, v)$ is the wind vector, $\vec{n}$ is the normal vector of wind. Then, RV in natural coordinates is transformed to

$$\begin{aligned} \zeta &= -\nabla_h \cdot \left(\left|\vec{V}\right| \vec{n}\right) = -\left(\partial_x, \partial_y\right) \cdot \left(-\left|\vec{V}\right| \sin\beta, \left|\vec{V}\right| \cos\beta\right) \\ &= -\left(\partial_x, \partial_y\right) \cdot (-v, u) = \frac{\partial v}{\partial x} - \frac{\partial u}{\partial y} \end{aligned} \tag{2}$$

where β is the vectorial angle between u-wind and v-wind vectors with $\sin\beta = \frac{v}{\left|\vec{V}\right|}$ and $\cos\beta = \frac{u}{\left|\vec{V}\right|}$.

In this way, SV can be expressed as

$$\begin{aligned} \zeta^s &= -\nabla_h \left|\vec{V}\right| \cdot \vec{n} = -\left(\frac{\partial \left|\vec{V}\right|}{\partial x}, \frac{\partial \left|\vec{V}\right|}{\partial y}\right) \cdot (-\sin\beta, \cos\beta) \\ &= \frac{v}{\left|\vec{V}\right|} \frac{\partial \left|\vec{V}\right|}{\partial x} - \frac{u}{\left|\vec{V}\right|} \frac{\partial \left|\vec{V}\right|}{\partial y} \end{aligned} \tag{3}$$

Then, the direct formula we used in this study to calculate CV is

$$\begin{aligned} \zeta^c &= -\left|\vec{V}\right| \nabla_h \cdot \vec{n} = -\left|\vec{V}\right| \left(\partial_x, \partial_y\right) \cdot (-\sin\beta, \cos\beta) \\ &= \left|\vec{V}\right| \left(\frac{\partial \sin\beta}{\partial x} - \frac{\partial \cos\beta}{\partial y}\right) = \left|\vec{V}\right| \left(\frac{\partial \frac{v}{\left|\vec{V}\right|}}{\partial x} - \frac{\partial \frac{u}{\left|\vec{V}\right|}}{\partial y}\right) \end{aligned} \tag{4}$$

This expression is further decomposed to

$$\begin{aligned} \zeta^c &= \left|\vec{V}\right| \left[\left(\frac{1}{\left|\vec{V}\right|} \frac{\partial v}{\partial x} - v \frac{1}{\left|\vec{V}\right|^2} \frac{\partial \left|\vec{V}\right|}{\partial x}\right) - \left(\frac{1}{\left|\vec{V}\right|} \frac{\partial u}{\partial y} - u \frac{1}{\left|\vec{V}\right|^2} \frac{\partial \left|\vec{V}\right|}{\partial y}\right)\right] \\ &= \left(\frac{\partial v}{\partial x} - \frac{\partial u}{\partial y}\right) - \left(\frac{v}{\left|\vec{V}\right|} \frac{\partial \left|\vec{V}\right|}{\partial x} - \frac{u}{\left|\vec{V}\right|} \frac{\partial \left|\vec{V}\right|}{\partial y}\right) = \zeta - \zeta^s \end{aligned} \tag{5}$$

showing the corresponding expression of Eq. (1) in rectangular coordinates.

The CV is a better representation of TEW and TC circulation than the RV[35] and is commonly used in TEW studies[32,33,36]. The circulation shown by RV has tilted shape (Supplementary Fig. S1A) and is asymmetric with respect to the TC center. This kind of asymmetry comes from the SV. After removing the SV from RV, the CV pattern shows a very symmetric and clear wave structure (Supplementary Fig. S1B).

TEW metrics

Here, we define the TEWs based on the convective condition, OLR, and the dynamical condition, CV at 900 hPa. We note that the dynamical profiles of TEW and TC genesis events peak at around 900 hPa (Supplementary Fig. S2), i.e., the characteristic level of their CV horizontal structure. For sensitivity test, we also check our results based on CV at 850 and 700 hPa in this study. TEWs climatology (Fig. 1A, B) is represented by the filtered OLR and CV seasonal 1-STD during June–October in the Northern Hemisphere and December–April in the Southern Hemisphere. OLR in the TD-band, which corresponds to westward propagating wavenumbers 6–20 and a period of 2–10 days, was retained by a wavenumber-frequency filter proposed by Wheeler and Kiladis[26]. The 6-hourly CV was daily averaged and radially averaged (500 km) at each grid point to filter out noise. Then, it was filtered using wavenumber-frequency filter method to isolate westward-moving activities which is same to processing the OLR. Further, based on the global pattern of TD-filtered OLR and CV seasonal standard deviation (Fig. 1A, B) and the averaged OLR and CV anomaly for all TC cases in each basin (Fig. 1C–H), the threshold of OLR anomaly is determined to be -10 W m^{-2} and CV anomaly $\pm 0.3 \times 10^{-5}$ s^{-1}.

MDR definition

The definition of AL MDR is 10–20°N and 20–80°W, following the initiatory definition in previous study[40]. The MDRs in the NI, WP, EP, SI, and SP are respectively 15–23°N and 65–95°E, 7–30°N and 10–160°E, 10–17°N and 90–150°W, 10–20°S and 40–136°E, and 12–20°S and 136°E–160°W.

TC movement direction

We define TC movement direction after genesis based on the angle between the location at 6 h after TC genesis and that of genesis location. If the angle is between 135 and 225 degrees, this TC case is considered to be moving westward and between 45 and 135 degrees poleward.

Data availability

All data used in this study are freely available at the following websites: ERA5: https://cds.climate.copernicus.eu; IBTrACS: https://www.ncei.noaa.gov/products/international-best-track-archive.

Code availability

Codes are available upon request. Figures were generated by Python 3.11.6 (Matplotlib 3.8.1 and Cartopy 0.21.1).

Received: 5 September 2024; Accepted: 18 March 2025;
Published online: 28 March 2025

References

1. Burpee, R. W. The Origin and Structure of Easterly Waves in the Lower Troposphere of North Africa. *J. Atmos. Sci.* **29**, 77–90 (1972).
2. Burpee, R. W. Characteristics of African Easterly Waves. *A Half Century of Progress in Meteorology: A Tribute to Richard Reed* 91–108, https://doi.org/10.1007/978-1-878220-69-1_7 (2003).
3. Brammer, A. & Thorncroft, C. D. Spatial and Temporal Variability of the Three-Dimensional Flow around African Easterly Waves. *Mon. Weather Rev.* **145**, 2879–2895 (2017).
4. Hollis, M. A., McCrary, R. R., Stachnik, J. P., Lewis-Merritt, C. & Martin, E. R. A global climatology of tropical easterly waves. *Clim. Dyn.* **1**, 1–16 (2023).
5. Burpee, R. W. Characteristics of North African Easterly Waves During the Summers of 1968 and 1969. *J. Atmos. Sci.* **31**, 1556–1570 (1974).
6. Wu, M. L. C., Reale, O., Schubert, S. D., Suarez, M. J. & Thorncroft, C. D. African easterly jet: Barotropic instability, waves, and cyclogenesis. *J. Clim.* **25**, 1489–1510 (2012).
7. Thorncroft, C. D. & Blackburn, M. Maintenance of the African easterly jet. *Q. J. R. Meteorological Soc.* **125**, 763–786 (1999).
8. Grogan, D. F. P., Nathan, T. R. & Chen, S. H. Structural Changes in the African Easterly Jet and Its Role in Mediating the Effects of Saharan Dust on the Linear Dynamics of African Easterly Waves. *J. Atmos. Sci.* **76**, 3351–3365 (2019).
9. Chen, T. C., Wang, S. Y. & Clark, A. J. North Atlantic Hurricanes Contributed by African Easterly Waves North and South of the African Easterly Jet. *J. Clim.* **21**, 6767–6776 (2008).
10. Ross, R. S., Krishnamurti, T. N. & Pattnaik, S. Interactions of diabatic heating in convective superbursts with energy conversion processes in the genesis of Cape Verde hurricanes from African easterly waves. *Mon. Weather Rev.* **140**, 748–773 (2012).
11. Cecelski, S. F. & Zhang, D. L. Genesis of hurricane julia (2010) within an african easterly wave: Low-level vortices and upper-level warming. *J. Atmos. Sci.* **70**, 3799–3817 (2013).
12. Bercos-Hickey, E., Nathan, T. R. & Chen, S. H. Effects of Saharan Dust Aerosols and West African Precipitation on the Energetics of African Easterly Waves. *J. Atmos. Sci.* **79**, 1911–1926 (2022).

13. Arnault, J. & Roux, F. Failed Cyclogenetic Evolution of a West African Monsoon Perturbation Observed during AMMA SOP-3. *J. Atmos. Sci.* **67**, 1863–1883 (2010).
14. Schwendike, J. & Jones, S. C. Convection in an African Easterly Wave over West Africa and the eastern Atlantic: A model case study of Helene (2006). *Q. J. R. Meteorological Soc.* **136**, 364–396 (2010).
15. Leppert, K. D., Petersen, W. A. & Cecil, D. J. Electrically active convection in tropical easterly waves and implications for tropical cyclogenesis in the atlantic and east pacific. *Mon. Weather Rev.* **141**, 542–556 (2013).
16. Semunegus, H., Mekonnen, A. & Schreck, C. J. Characterization of convective systems and their association with African easterly waves. *Int. J. Climatol.* **37**, 4486–4492 (2017).
17. Núñez Ocasio, K. M., Evans, J. L. & Young, G. S. A Wave-Relative Framework Analysis of AEW–MCS Interactions Leading to Tropical Cyclogenesis. *Mon. Weather Rev.* **148**, 4657–4671 (2020).
18. Beven, J. L. et al. Atlantic Hurricane Season of 2005. *Mon. Weather Rev.* **136**, 1109–1173 (2008).
19. Russell, J. O., Aiyyer, A., White, J. D. & Hannah, W. Revisiting the connection between African Easterly Waves and Atlantic tropical cyclogenesis. *Geophys. Res. Lett.* **44**, 587–595 (2017).
20. Landsea, C. W. A Climatology of Intense (or Major) Atlantic Hurricanes. *Mon. Weather Rev.* **121**, 1703–1713 (1993).
21. Patricola, C. M., Saravanan, R. & Chang, P. The Response of Atlantic Tropical Cyclones to Suppression of African Easterly Waves. *Geophys. Res. Lett.* **45**, 471–479 (2018).
22. Danso, D. K., Patricola, C. M. & Bercos-Hickey, E. Influence of African Easterly Wave Suppression on Atlantic Tropical Cyclone Activity in a Convection-Permitting Model. *Geophys. Res. Lett.* **49**, e2022GL100590 (2022).
23. Bercos-Hickey, E. & Patricola, C. M. The Effects of African Easterly Wave Suppression by Wave Track on Atlantic Tropical Cyclones. *Geophys. Res. Lett*. **50**, e2023GL105491 (2023).
24. Serra, Y. L., Kiladis, G. N. & Cronin, M. F. Horizontal and Vertical Structure of Easterly Waves in the Pacific ITCZ. *J. Atmos. Sci.* **65**, 1266–1284 (2008).
25. Serra, Y. L., Kiladis, G. N. & Hodges, K. I. Tracking and Mean Structure of Easterly Waves over the Intra-Americas Sea. *J. Clim.* **23**, 4823–4840 (2010).
26. Wheeler, M. & Kiladis, G. N. Convectively Coupled Equatorial Waves: Analysis of Clouds and Temperature in the Wavenumber–Frequency Domain. *J. Atmos. Sci.* **56**, 374–399 (1999).
27. Schreck, C. J., Molinari, J. & Mohr, K. I. Attributing Tropical Cyclogenesis to Equatorial Waves in the Western North Pacific. *J. Atmos. Sci.* **68**, 195–209 (2011).
28. Schreck, C. J., Molinari, J. & Aiyyer, A. A Global View of Equatorial Waves and Tropical Cyclogenesis. *Mon. Weather Rev.* **140**, 774–788 (2012).
29. Frank, W. M. & Roundy, P. E. The Role of Tropical Waves in Tropical Cyclogenesis. *Mon. Weather Rev.* **134**, 2397–2417 (2006).
30. Feng, T. et al. Synoptic-Scale Waves in Sheared Background Flow over the Western North Pacific. *J. Atmos. Sci.* **73**, 4583–4603 (2016).
31. Wu, L. & Takahashi, M. Contributions of tropical waves to tropical cyclone genesis over the western North Pacific. *Clim. Dyn.* **50**, 4635–4649 (2018).
32. Brammer, A. & Thorncroft, C. D. Variability and Evolution of African Easterly Wave Structures and Their Relationship with Tropical Cyclogenesis over the Eastern Atlantic. *Mon. Weather Rev.* **143**, 4975–4995 (2015).
33. Belanger, J. I., Jelinek, M. T. & Curry, J. A. A climatology of easterly waves in the tropical Western Hemisphere. *Geosci. Data J.* **3**, 40–49 (2016).
34. Lewis-Merritt, C., Stachnik, J. P., Hollis, M. A., Martin, E. R. & McCrary, R. R. A Global Climatology of Diabatic Heating in Tropical Easterly Waves. *J. Clim.* **1**, 2081–2101 (2024).
35. Berry, G., Thorncroft, C. & Hewson, T. African Easterly Waves during 2004—Analysis Using Objective Techniques. *Mon. Weather Rev.* **135**, 1251–1267 (2007).
36. Torres, V. M. & Thorncroft, C. D. Interdecadal Variability of Easterly Waves Over the Tropical Northeastern Pacific. *Geophys Res Lett.* **49**, e2022GL099090 (2022).
37. Hersbach, H. et al. *ERA5 Hourly Data on Pressure Levels from 1940 to Present [Accessed on 12-Jun-2024]*. (Copernicus Climate Change Service (C3S) Climate Data Store (CDS), 2023).
38. Gahtan, J. et al. *International Best Track Archive for Climate Stewardship (IBTrACS) Project, Version 4r01. [Subset Since1980 Accessed on 16-Nov-2024]. NOAA National Centers for Environmental Information* (NOAA National Centers for Environmental Information, 2024).
39. Knapp, K. R., Kruk, M. C., Levinson, D. H., Diamond, H. J. & Neumann, C. J. The International Best Track Archive for Climate Stewardship (IBTrACS): Unifying Tropical Cyclone Data. *Bull. Am. Meteorol. Soc.* **91**, 363–376 (2010).
40. Van den Dool, H. M. et al. Seasonal-to-Decadal Predictability and Prediction of North American Climate—The Atlantic Influence. *J. Clim.* **19**, 6005–6024 (2006).
41. Feng, X., Yang, G. Y., Hodges, K. I. & Methven, J. Equatorial waves as useful precursors to tropical cyclone occurrence and intensification. *Nat. Commun.* **14**, 1–11 (2023).
42. Yang, G. Y., Methven, J., Woolnough, S., Hodges, K. & Hoskins, B. Linking African Easterly Wave Activity with Equatorial Waves and the Influence of Rossby Waves from the Southern Hemisphere. *J. Atmos. Sci.* **75**, 1783–1809 (2018).
43. Berry, G. J., Reeder, M. J. & Jakob, C. Coherent Synoptic Disturbances in the Australian Monsoon. *J. Clim.* **25**, 8409–8421 (2012).
44. Fink, A. H. & Reiner, A. Spatiotemporal variability of the relation between African Easterly Waves and West African Squall Lines in 1998 and 1999. *J. Geophys. Res. Atmos.* **108**, 4332 (2003).
45. Russell, J. O. H. & Aiyyer, A. The Potential Vorticity Structure and Dynamics of African Easterly Waves. *J. Atmos. Sci.* **77**, 871–890 (2020).
46. Rajasree, V. P. M. et al. Tropical cyclogenesis: Controlling factors and physical mechanisms. *Tropical Cyclone Res. Rev.* **12**, 165–181 (2023).
47. Dunkerton, T. J., Montgomery, M. T. & Wang, Z. Tropical cyclogenesis in a tropical wave critical layer: Easterly waves. *Atmos. Chem. Phys.* **9**, 5587–5646 (2009).
48. Gallina, G. M. & Velden, C. S. Environmental vertical wind shear and tropical cyclone intensity change utilizing enhanced satellite derived wind information. In *25th Conf. on Hurricanes and Tropical Meteorology.* 172–173 (American Meteor Society, San Diego, CA, 2002).
49. Wong, M. L. M. & Chan, J. C. L. Tropical Cyclone Intensity in Vertical Wind Shear. *J. Atmos. Sci.* **61**, 1859–1876 (2004).
50. Wang, Z., Montgomery, M. T. & Dunkerton, T. J. Genesis of Pre–Hurricane Felix (2007). Part I: The Role of the Easterly Wave Critical Layer. *J. Atmos. Sci.* **67**, 1711–1729 (2010).
51. Núñez Ocasio, K. M. & Rios-Berrios, R. African Easterly Wave Evolution and Tropical Cyclogenesis in a Pre-Helene (2006) Hindcast Using the Model for Prediction Across Scales-Atmosphere (MPAS-A). *J. Adv. Model Earth Syst.* **15**, e2022MS003181 (2023).
52. Núñez Ocasio, K. M., Davis, C. A., Moon, Z. L. & Lawton, Q. A. Moisture Dependence of an African Easterly Wave Within the West African Monsoon System. *J. Adv. Model Earth Syst.* **16**, e2023MS004070 (2024).
53. Hsieh, J. S. & Cook, K. H. A Study of the Energetics of African Easterly Waves Using a Regional Climate Model. *J. Atmos. Sci.* **64**, 421–440 (2007).

54. Diaz, M. & Aiyyer, A. Absolute and Convective Instability of the African Easterly Jet. *J. Atmos. Sci.* **72**, 1805–1826 (2015).
55. Hsieh, J. S. & Cook, K. H. On the Instability of the African Easterly Jet and the Generation of African Waves: Reversals of the Potential Vorticity Gradient. *J. Atmos. Sci.* **65**, 2130–2151 (2008).
56. White, J. & Aiyyer, A. African easterly waves in an idealized general circulation model: instability and wave packet diagnostics. *Weather Clim. Dyn.* **2**, 311–329 (2021).
57. Russell, J. O. H., Aiyyer, A. & Dylan White, J. African Easterly Wave Dynamics in Convection-Permitting Simulations: Rotational Stratiform Instability as a Conceptual Model. *J. Adv. Model Earth Syst.* **12**, e2019MS001706 (2020).
58. Sobel, A. H. & Bretherton, C. S. Development of Synoptic-Scale Disturbances over the Summertime Tropical Northwest Pacific. *J. Atmos. Sci.* **56**, 3106–3127 (1999).
59. Li, T. Origin of the Summertime Synoptic-Scale Wave Train in the Western North Pacific. *J. Atmos. Sci.* **63**, 1093–1102 (2006).
60. Tam, C. Y. & Li, T. The Origin and Dispersion Characteristics of the Observed Tropical Summertime Synoptic-Scale Waves over the Western Pacific. *Mon. Weather Rev.* **134**, 1630–1646 (2006).
61. Wolding, B. et al. Interactions between Moisture and Tropical Convection. Part I: The Coevolution of Moisture and Convection. *J. Atmos. Sci.* **77**, 1783–1799 (2020).
62. Núñez Ocasio, K. M., Brammer, A., Evans, J. L., Young, G. S. & Moon, Z. L. Favorable Monsoon Environment over Eastern Africa for Subsequent Tropical Cyclogenesis of African Easterly Waves. *J. Atmos. Sci.* **78**, 2911–2925 (2021).
63. Núñez Ocasio, K. M., Evans, J. L. & Young, G. S. Tracking mesoscale convective systems that are potential candidates for tropical cyclogenesis. *Mon. Weather Rev.* **148**, 655–669 (2020).
64. Hersbach, H. et al. *ERA5 Hourly Data on Single Levels from 1940 to Present [Accessed on 09-Nov-2024]*. (Copernicus Climate Change Service (C3S) Climate Data Store (CDS), 2023).
65. Viúdez, Á. & Haney, R. L. On the Shear and Curvature Vorticity Equations. *J. Atmos. Sci.* **53**, 3384–3394 (1996).

Acknowledgements

This research was supported by the Hong Kong Research Grants Council Early Career Scheme (9048309) and the National Natural Science Foundation of China (9240162).

Author contributions

J.-E.C. conceived the idea. X.Q.D. conducted the data analysis, drafted the manuscript, and designed the figures. X.Q.D., J.-E.C., F.-F.J., and H.M.C. reviewed and edited the manuscript.

Competing interests

The authors declare no competing interests.

Additional information

Supplementary information The online version contains supplementary material available at https://doi.org/10.1038/s41612-025-01014-y.

Correspondence and requests for materials should be addressed to Jung-Eun Chu.

Reprints and permissions information is available at http://www.nature.com/reprints

Publisher's note Springer Nature remains neutral with regard to jurisdictional claims in published maps and institutional affiliations.

Open Access This article is licensed under a Creative Commons Attribution-NonCommercial-NoDerivatives 4.0 International License, which permits any non-commercial use, sharing, distribution and reproduction in any medium or format, as long as you give appropriate credit to the original author(s) and the source, provide a link to the Creative Commons licence, and indicate if you modified the licensed material. You do not have permission under this licence to share adapted material derived from this article or parts of it. The images or other third party material in this article are included in the article's Creative Commons licence, unless indicated otherwise in a credit line to the material. If material is not included in the article's Creative Commons licence and your intended use is not permitted by statutory regulation or exceeds the permitted use, you will need to obtain permission directly from the copyright holder. To view a copy of this licence, visit http://creativecommons.org/licenses/by-nc-nd/4.0/.

© The Author(s) 2025